Large-area ordered polymeric nanochannel arrays - a high-resolution investigation

P. Müller-Buschbaum[1], E. Bauer[1], E. Maurer[1], K. Schlögl[1], S.V. Roth[2], R. Gehrke[2]

[1]TU München, Physik-Department, LS E13, James-Franck-Str.1, 85747 Garching (Germany)
[2]HASYLAB at DESY, Notkestr. 85, 22603 Hamburg (Germany)

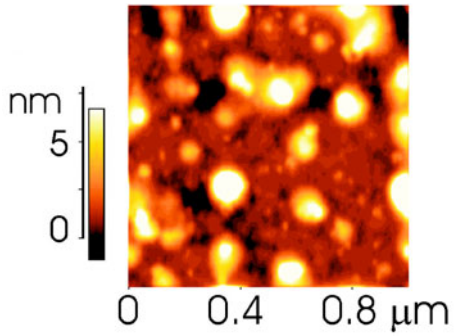

Large scale arrays of polymer nanochannels are important tools for many applications, such as micro-fluidics and fabrication of bioanalytical assays. Polymer nanochannels are defined as the alignment of polymeric material in walls with negligible interconnection in perpendicular direction. We present here a new, unexplored route to create such polymeric arrays. Their large-scale order as well as their orientation with respect to the underlying substrate is probed using high-resolution grazing incidence small-angle x-ray scattering.

(Published in: Appl. Phys. Lett. **88** 083114 (2006))

Nanochannel array applications and preparation

The ability to nanostructure polymer interfaces is of great importance in many areas of basic and technological applications. To name just a few are organic electronics, microelectronics, combinatorial biotechnology and nano- and microfluidics. The main techniques used for fabrication are "top-down" and "bottom-up". In our present study we focused on a new, easy approach to create a large-scale nanochannel array. The array was prepared as follows. A 100%-cellulose based fuzz free wipe [1] was soaked with iso-propanol-PDMS solution (concentration <0.1 mg/ml). The glass slide (surface roughness <0.5 nm) was treated with this wipe and kept electro-statically isolated during the treatment. The contact pressure was (24±3)kPa. The wiping direction was along the long side of the glass slide. The solvent evaporates at temperature-controlled climatized con-ditions. The PDMS dewets the glass surface [2,3]. Induced by directional deposition and evaporation, the nanostructure is frozen in. Due to the low concentration, only a very small amount of PDMS is transferred to the glass slide.

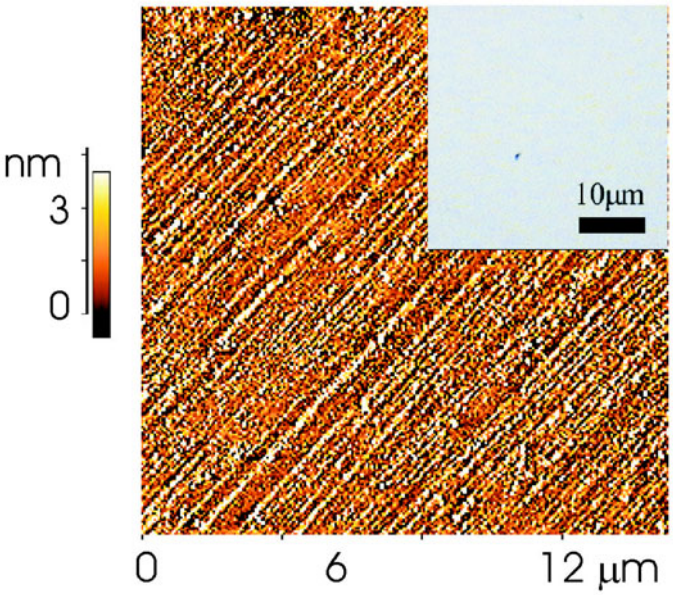

Figure 1. Real space structural data of the PDMS nano-channels: AFM topography data with 15x15µm^2 scan range and optical micrograph in the inset. Reproduced with permission from Appl. Phys. Lett. **88**, 083114 (2006). Copyright 2006, American Institute of Physics.

Sample characterization with local methods

Real space images from the sample were obtained using atomic force microscopy (AFM). Additionally, optical micrograph pictures were taken. As can be seen from the inset in figure 1 the surface seems to be featureless in the optical regime and cannot be distinguished from the untreated

glass surface. The AFM image in figure 1, however, clearly shows an oriented structure. A zooming-in is shown in figure 2. In figure 2b, polymeric walls are clearly visible. Interconnections between adjacent walls are missing; hence this structure fulfils all the prerequisites for a nanochannel array. A line scan in figure 2c allows extracting the geometry of the nanochannels:

Their height is 3 nm, their mean distance D= 166 nm. The Fourier-transform of figure 2b is shown in figure 2d. The high ordering of the nanochannels is corroborated by the two streaking signals. For comparison, figure 2a shows the resulting structure without wiping. Only a dewetted structure consisting of polydisperse PDMS droplets is present.

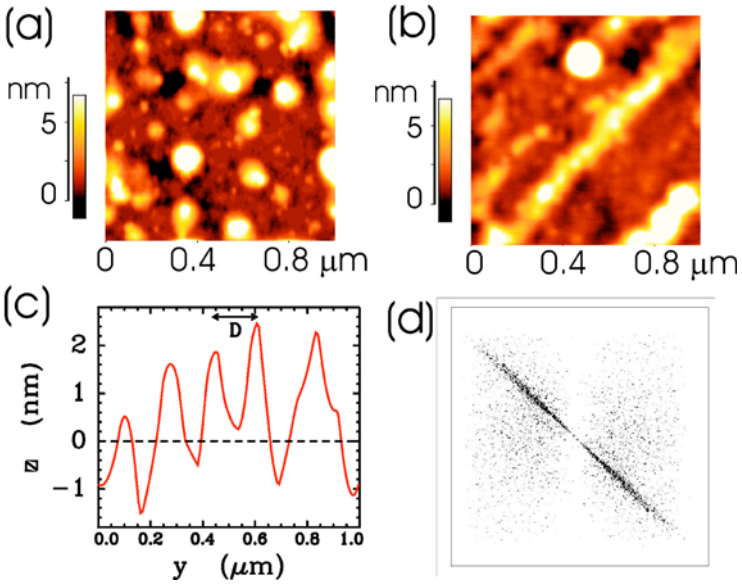

Figure 2. a) Dewetting structure resulting without wiping. b) Zoomed-in AFM data of fig. 1 with 1x1 µm^2 scan range demonstrating imperfections of the PDMS nanochannels. c) Representative line scan (D= 166 nm). d) Fourier transformed calculated from the AFM data. Reproduced with permission from Appl. Phys. Lett. **88**, 083114 (2006). Copyright 2006, American Institute of Physics.

High-resolution grazing incidence small-angle x-ray scattering

To probe the existence of the polymer nanochannel array over the whole substrate surface, we installed a high-resolution grazing incidence small-angle x-ray scattering (high-resolution GISAXS) at the beamline BW4 of HASYLAB [5], see figure 3. The wavelength chosen was λ= 1.38Å.

Experimental requirements for high-resolution GISAXS are in principle coupled with the beamline optics as well as with the way the GISAXS experiment is performed: Despite the strong differences in the intensity between the diffusely scattered intensity carrying the desired information about the lateral sample surface structure and the specularly reflected intensity, the use of a two-dimensional detector is very advantageous for any GISAXS experiment. Because the specular peak, broadened by the experimental resolution function, is only helpful for alignment purpose, in the GISAXS experiment it is shielded with a beamstop [6], which resembles a similarity to the common SAXS experiments in which the direct beam has to be shielded from the same reasons as well. However, whereas in SAXS the intensity carrying information about large bulk sample structures is located very close to this beamstop at small q-values, in GISAXS the Yoneda wing and the specular peak (shielded with a beamstop) can be separated due to the reflection geometry [7]. As a consequence, mainly three different types of GISAXS experiments can be distinguished from the relative position of the Yoneda wing (located at the critical angle α_c of the material under investigation) and specular peak [8].

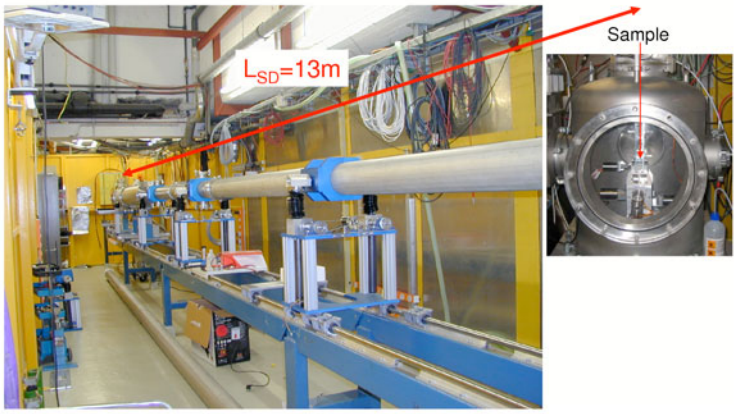

Figure 3. Photograph of the BW4-beamline. Visible is the long, segmented tube. The inset shows the full-vacuum-GISAXS-setup.

In the GISAXS experiment of first type, the incident angle fulfils $\alpha_i<\alpha_c$ and consequently on the detector the specular peak appears at $\alpha_f=\alpha_i<\alpha_c$ below the Yoneda wing at $\alpha_f=\alpha_c$. Depending on the experimental resolution this will enable a separation of both signals along the α_f-axis (or q_z-axis) of the detector and thus a proper separation of the diffuse and the specular scattering, which is essential for the GISAXS analysis (see examples within this article [8]). Within the present set-up the incident angle was chosen as $\alpha_i=0.01°$. Additionally, a very large sample-to-detector distance of $L_{SD}=13$m was chosen. This setup enables to detect length scales from 35 nm up to theoretically 21µm. In this experiment a maximum resolution of $2.75\text{x}10^{-4}\text{nm}^{-1}$ was achieved. Due to the very shallow incident angle, specular and direct beam can be blocked by one beamstop. The Yoneda peak, being very surface-structure sensitive due to its interference nature, is well separated. Consequently, specular and diffuse scattering are easily separated.

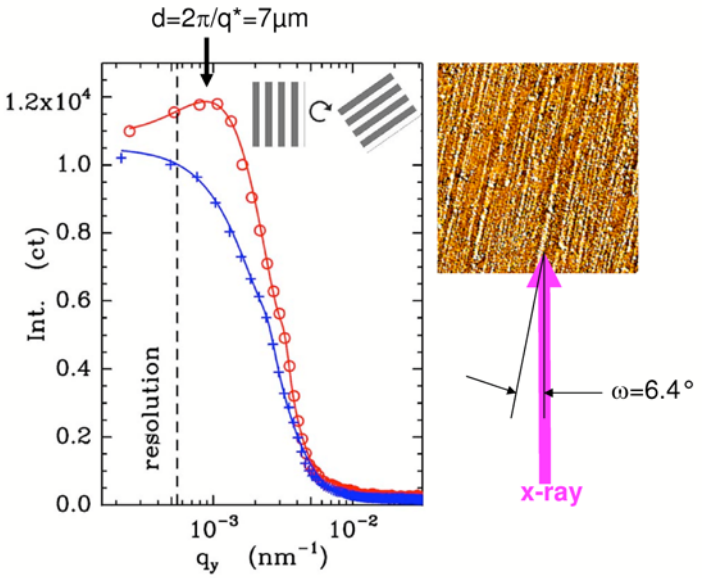

Figure 4. GISAXS data of the glass surface with PDMS nanochannels on top (circles) in comparison with data of a bare glass surface (crosses). The arrow at q_y^p marks a position related to the structure factor of the tilted nanochannels. The dashed line indicates the resolution limit. The inset visualizes the rotation of the nanochannel array by ω with respect to the x-ray beam (dotted line). Reproduced with permission from Appl. Phys. Lett. **88**, 083114 (2006). Copyright 2006, American Institute of Physics.

Moreover, at $\alpha_i=0.01°$ the penetration depth of the x-rays is minimal, hence a clear signal from the weakly scattering PDMS-array is achieved. On the other hand due to the projection of the beam onto the footprint, the whole sample surface is illuminated. This is a prerequisite to prove the homogeneity of the nanochannel array.

Results

From the 2D intensity distribution the chemical composition of thin films as well as the length scales parallel to the substrate surface can be deduced [6]. The wavevector transfer is decomposed in two components, q_z and q_y, both perpendicular to the incoming beam. While q_z probes the length scales perpendicular to the sample surface, the intensity distribution for a slice along q_y is governed by the lateral length scales present. The most prominent feature along q_z beside the specular beam is the Yoneda peak. This maximum originates from the interference of incoming and reflected wave, when the incident angle α_i or exit angle α_f equal the critical angle of the materials present. Due to the interference, the Yoneda peak is most sensitive to the surface morphology and structure. Hence we show in figure 4 the intensity distribution along q_y for the out-of-plane cut at the critical angle of PDMS. For comparison, the identical cut of the bare glass substrate is shown. The dotted line denotes the resolution. At q_y^p a maximum is clearly visible. This maximum corresponds to a most-prominent in-plane length scale of $\Lambda=7$µm. Using [9, 10] $\alpha_i \approx 0$ and $q_x=(2\pi / \lambda)[\cos\alpha_f-\cos\alpha_i]$ being the wavevector transfer parallel to the incident beam, one derives a condition for the position of the zero order maximum:

$$q_y^p + \frac{q_x}{\tan\omega} = 0 \Leftrightarrow \tan\omega = -\frac{\pi}{\lambda}\frac{\alpha_f^2}{q_y^p}$$

ω denotes the orientation of the nanochannel array with respect to the long edge of the glass substrate. This formula takes into account the finite curvature of the Ewald-sphere which leads to coupling of the two wavevector components q_y and q_x parallel to the sample surface. This, in combination with the finite tilt ω, leads to a virtual enlarged period of the nanochannel array.

Conclusion

We have proven a new and simple route to create large area shallow polymeric nanochannel arrays under the mechanical and ambient conditions mentioned above, which might be interesting for future applications in micro- and nanofluidics. Using a very high-resolution GISAXS setup at BW4 we investigate the extremely weak scattering array and are able to the homogeneity of the nanochannel array over the whole substrate (86x20 mm^2) as well as its tilt of $\omega = 6.4^o$ with respect to the long edge of the glass substrate. With one zero-order scattering maximum present, the preparation process is not as perfect as lithographic, interference, diblock polymer or external-field methods [11-21]. However, its simplicity allows for easy scaling and time-reduced preparation of well controlled surface patterns.

Acknowledgement

This work was financially supported by the DFG Schwerpunktprogramm SPP 1164 "Nano- and Microfluidics" (Mu1487/2).

References

[1] KIMWIPES Lite, Kimberly Clark
[2] P. Müller-Buschbaum, J.Phys.Condens.Matter **15**, R1549 (2003).
[3] I. Karapanagiotis, D.F. Evans, W.W. Gerberich, Colloids Surf. A **207**, 59 (2002).
[4] P. Müller-Buschbaum, E. Bauer, O. Wunnicke, M. Stamm, J.Phys.Condens.Matter **17**, S363 (2005).
[5]} S.V. Roth, R. Döhrmann, M. Dommach, M. Kuhlmann, I. Kröger, R. Gehrke, H. Walter, C. Schroer, B. Lengeler, P. Müller-Buschbaum, Rev. Sci. Instr. **77**, 085106 (2006).
[6] P. Müller-Buschbaum, Anal. Bioanal. Chem. **376**, 3 (2003).
[7] P. Müller-Buschbaum, M. Casagrande, J.S. Gutmann, T. Kuhlmann, M. Stamm, S. Cunis, G. von Krosigk, U. Lode, R. Gehrke, Europhys. Lett. **42**, 517 (1998).
[8] P. Müller-Buschbaum, Prog. Col. Polym. Sci. **132**, 23 (2006).
[9] T. Salditt, H. Rhan, T.H. Metzger, J. Peisl, R. Schuster, J.P. Kotthaus, Z. Phys. B **96**, 227 (1994).
[10] D. Le Bolloch, F. Livet, F. Bley, T. Schulli, M. Veron, T.H. Metzger, J. Synchrotron Rad. **9**, 258
[11] L. Peters, Semiconductor internat. **38**, 28 (2005).
[12] Z. Yu, S.Y. Chou, Nano Lett. **4**, 341 (2004).
[13] A. Fahmi, M. Stamm, Langmuir **21**, 1062 (2005).
[14] Q. Lu, C. G. Bazuin, Nano Lett **5**, 1309 (2005).
[15] T. Thurn-Albrecht, J. Schotter, G.A. Kästle, N. Emley, T. Shibauchi, L. Krusin-Elbaum, K. Guarini, C.T. Black, M.T. Tuominen, T.P. Russell, Science **290**, 2126 (2000).
[16] X. Yan, F. Liu, Z. Li, G. Liu, Macromolecules **34**, 9112 (2001).
[17] J.P. Spatz, M. Möller, M. Noeske, R.J. Behm, M. Pietralla, Macromolecules **30**, 3874 (1997).
[18] E. Bormashenko, R. Pogreb, O. Stanevsky, Y. Bormashenko, T. Stein, V.-Z. Gaisin, R. Cohen, O.V. Gendelman, Macromol. Mater. Eng. **290**, 114 (2005).
[19] L.J. Guo, X. Cheng, C.F. Chou, Nano Lett. **4**, 69 (2004).
[20] C. Lee, E.H. Yang, N.V. Myung, T. George, Nano Lett. **3**, 1339 (2003).
[21] N.R. Tas, J.W. Berenschot, P. Mela, H.V. Jansen, M. Elwenspoek, A. van den Berg Nano Lett. **2**,1031 (2002).